Article

Current Biology

Ecophysical constraints on avian adaptation and diversification

Graphical abstract

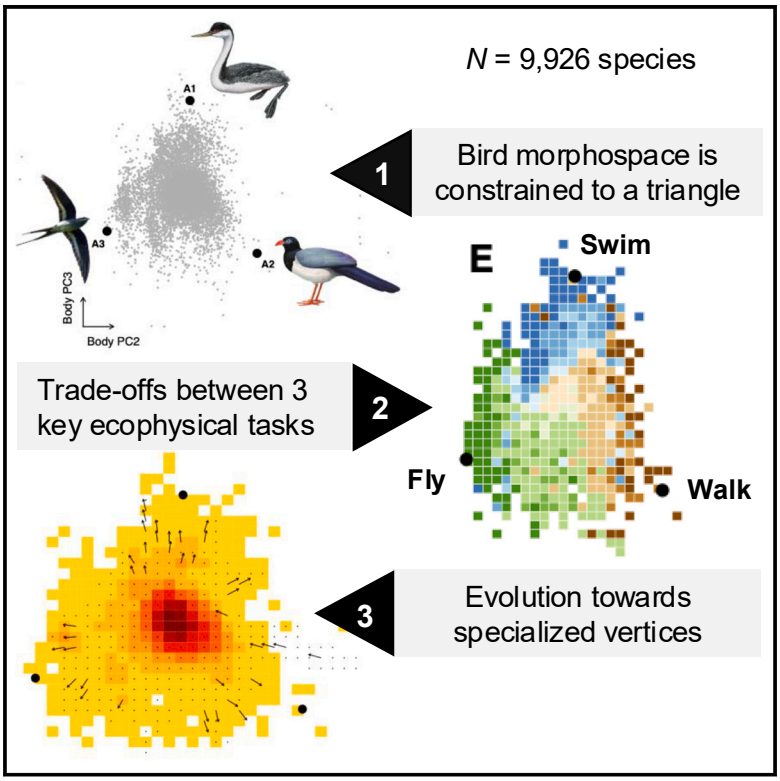

Highlights

- Variation in the beak and body shape of birds is constrained in trait space
- Fundamental trade-offs between physical tasks explain morphological constraints
- Extreme morphologies appear to reflect specialization on single physical tasks
- Evolution trends toward specialized extremes, where extinction risk may increase

Authors

Ferran Sayol, Bouwe R. Reijenga, Joseph A. Tobias, Alex L. Pigot

Correspondence

fsayol@gmail.com

In brief

Sayol et al. show bird morphological diversity is constrained by trade-offs among key physical tasks for feeding and locomotion, with evolution trending toward specialized forms at the vertices of the resulting triangular morphospace. The structure and dynamics of morphological diversity may thus follow from relatively simple ecophysical rules.

Sayol et al., 2025, Current Biology *35*, 1–11
March 24, 2025
https://doi.org/10.1016/j.cub.2025.02.015

CellPress

Please cite this article in press as: Sayol et al., Ecophysical constraints on avian adaptation and diversification, Current Biology (2025), https://doi.org/10.1016/j.cub.2025.02.015

Current Biology

CellPress

Article

Ecophysical constraints on avian adaptation and diversification

Ferran Sayol,[1,2,5,*] Bouwe R. Reijenga,[2,3] Joseph A. Tobias,[4] and Alex L. Pigot[2]
[1]CREAF, Cerdanyola del Vallès 08193, Spain
[2]Centre for Biodiversity and Environment Research, Department of Genetics, Evolution and Environment, University College London, London WC1E 6BT, UK
[3]Department of Earth Sciences, University of Oxford, Oxford OX1 3AN, UK
[4]Department of Life Sciences, Imperial College London, Silwood Park, Ascot SL5 7PY, UK
[5]Lead contact
*Correspondence: fsayol@gmail.com
https://doi.org/10.1016/j.cub.2025.02.015

SUMMARY

The evolution of morphological diversity is ultimately governed by physical laws and ecological contexts, which together impose a range of ecophysical constraints. Substantial progress has been made in identifying how these constraints shape the form and function of producers (plants), but similar knowledge is lacking for consumers, in part because the requisite data have not been available at sufficient scale for animals. Using morphometric measurements for all birds, we demonstrate that observed variation is restricted—both for beak shape and body shape—to triangular regions of morphospace with clearly defined boundaries and vertices (corners). By combining morphometric data with information on ecological and behavioral functions, we provide evidence that the extent of avian morphospace reflects a trade-off between three fundamental physical tasks for feeding (crush, engulf, and reach) that characterize resource acquisition and processing by the beak and three physical tasks (fly, swim, and walk) that characterize avian lifestyles or locomotion. Phylogenetic analyses suggest that trajectories of morphological evolution trend toward the vertices, with lineages evolving from a core of functional generalists toward more specialized physical tasks. We further propose that expansion beyond the current boundaries of morphospace is constrained by the shorter evolutionary lifespan of functional specialists, although patterns of speciation rate and current extinction risk provide only weak support for this hypothesis. Overall, we show that the structure of avian morphospace follows relatively simple rules defined by ecophysical constraints and trade-offs, shedding light on the processes shaping modern animal diversity and responses to environmental change.

INTRODUCTION

Over billions of years of evolution, life has explored an enormous diversity of physical forms. This morphological diversity largely reflects the variety of different strategies employed by organisms for capturing and allocating resources and for exploiting environments with radically different physical states and properties.[1–5] Yet, the range of morphological forms in existence often seems highly constrained in comparison to all geometrically possible options.[6,7] Explanations for the limits to morphological diversity tend to focus on genetic constraints, developmental limitations, or historical contingency,[8] placing less emphasis on constraints relating to the physical environment. Nonetheless, all organisms must ultimately abide by the universal laws of physics,[9,10] imposing bounds on the range and combination of traits that are biomechanically possible given a particular body plan and that are viable in a world of relentless competition and selection.[8,11,12] Understanding the strength, nature, and identity of these physical constraints is essential not only for explaining the evolution of phenotypic diversity within and across species,[13,14] but also for predicting the adaptive capacity and resilience of populations under rapid environmental change.[15,16] However, despite this fundamental importance, we lack a comprehensive understanding of how the physical environment organizes and limits the diversity of morphological forms observed in nature, especially among heterotrophic animals that comprise much of global biodiversity.

Constraints to evolution imposed by the physical environment (i.e., ecophysical constraints) are expected to lead to regular patterns in the distribution of morphological forms, shapes, and structures of organisms across multivariate trait space, or "morphospace."[17,18] In particular, because organisms are subject to multiple physical constraints, this results in fundamental trade-offs, with improved performance in one functional task coming at the expense of weaker performance in other tasks.[7,19] In this case, natural selection is expected to optimize organismal performance across these multiple tasks, eliminating combinations of traits where overall performance is reduced and favoring morphological solutions that align along a limited number of independent dimensions.[17] The co-variation between multiple aspects of organism function and body size represents one such axis along which morphological diversity is organized.[20,21] The

Please cite this article in press as: Sayol et al., Ecophysical constraints on avian adaptation and diversification, Current Biology (2025), https://doi.org/10.1016/j.cub.2025.02.015

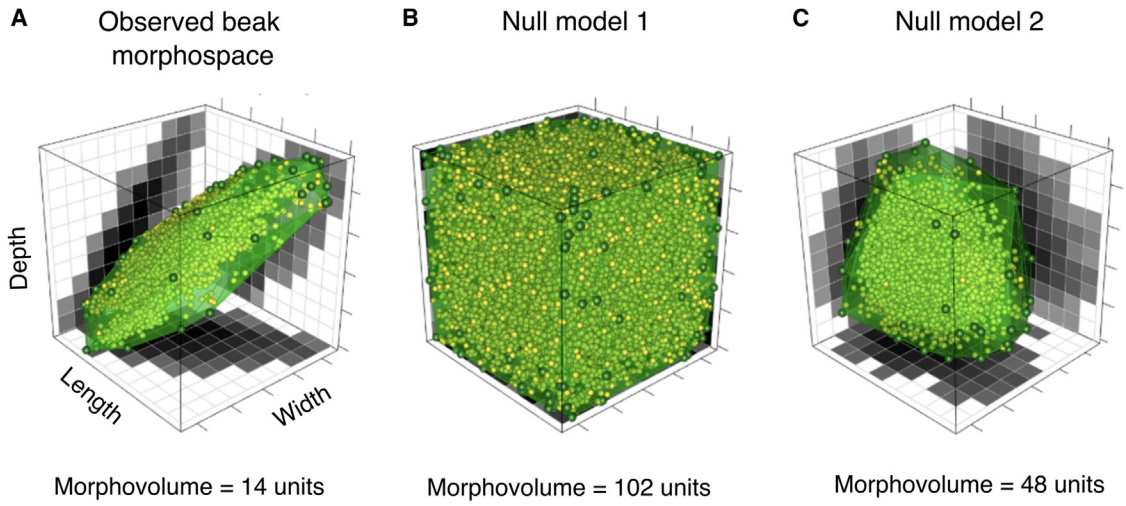

Figure 1. The volume and shape of avian beak morphospace

(A) Empirical beak morphospace and (B and C) alternative null models of morphospace occupation are shown. Points show species (n = 9,942) in 3D beak space defined by beak length, width, and depth measurements. Green polygons show the boundary of the convex hull enclosing all species, with dark green points indicating the vertices of the hull. The density of species is projected onto each 2D plane. Dark shading indicates a higher density. (B) Null model 1 assumes there are no trade-offs among beak trait dimensions or selection against extreme beak forms. (C) Null model 2 assumes beak trait dimensions vary independently, but extreme beak forms are not viable. The volume of morphospace occupied by real beaks and each null model is indicated.
See also Figure S1.

advent of large-scale datasets characterizing whole-organism plant form has identified additional axes of constraint acting on photosynthesizing primary producers,[22,23] providing an organizing framework for understanding and predicting how autotrophic species and communities respond to environmental change.[1,24,25] By contrast, due to a lack of quantitative morphological data, the search for the key constraints and trade-offs shaping the evolution of morphological diversity across higher trophic levels has lagged far behind, despite the critical role of these organisms in driving ecosystem processes and supporting plant diversity.[26,27]

Here, we test for constraints on the morphospace occupied by birds, which, despite conservatism in their body plan, have radiated across multiple trophic levels and physical environments.[2] Exceptionally, owing to recent sampling efforts, quantitative data are now comprehensively available for a number of key morphological traits, allowing us to characterize the size and shape of morphospace occupied by almost all ~10,000 extant bird species.[28] We initially focus on variation in the beak, the primary anatomical apparatus used by birds for resource acquisition and processing, which offers a model system for understanding the functional, developmental, and genetic basis of trait variation.[29–31] We use the term "function" in its broadest sense to mean the action of a morphological trait.[32]

Using linear measurements of beak length, width, and depth, we first characterize the volume and geometry of beak morphospace. We demonstrate that beaks occupy a highly restricted volume of what is geometrically possible, with variation in beak shape largely restricted to a triangular region of morphospace that reflects trade-offs among three main physical tasks required for acquiring and processing resources. Using measurements of the tail, wing, and tarsus, we show that variation in bird body shape is similarly restricted to a triangular region of morphospace, reflecting trade-offs among optimal modes of locomotion through different physical environments. Finally, we explore the macroevolutionary flux of lineages through morphospace to assess how ecophysical constraints and trade-offs have shaped avian diversity over deeper timescales, viewed through the lens of speciation rates and extinction risk.[33–37] The overall goal is to evaluate whether ecophysical rules provide a potential framework for understanding the evolution of morphological diversity and species resilience to global environmental change.

RESULTS AND DISCUSSION

Global beak morphospace

Based on log-transformed linear measurements of beak length, width, and depth, we used the convex hull enclosing all species to calculate the volume and shape of a 3D beak morphospace occupied by birds (Figure 1A). We compared this to two different null models that make contrasting assumptions about how species could be distributed throughout beak morphospace. Null model 1 assumes that trade-offs are absent and that within the observed extremes any combination of traits is equally viable. This leads to a morphospace resembling a cube (Figure 1B). We found that real beaks only occupy 14% of the volume of morphospace expected under null model 1 (Figure S1A), indicating that covariance among beak traits and/or selection against extreme trait combinations (i.e., the minimum or maximum values of multiple traits in the same species) limits the variety of beak forms. A higher covariance among traits is clearly the major factor because, despite exhibiting more extreme trait values, real beaks only occupy 29% of the volume of morphospace expected under null model 2, in which traits vary independently but where extreme trait combinations are not permitted (Figures 1C and S1A). In other words, trade-offs among traits,

Please cite this article in press as: Sayol et al., Ecophysical constraints on avian adaptation and diversification, Current Biology (2025), https://doi.org/10.1016/j.cub.2025.02.015

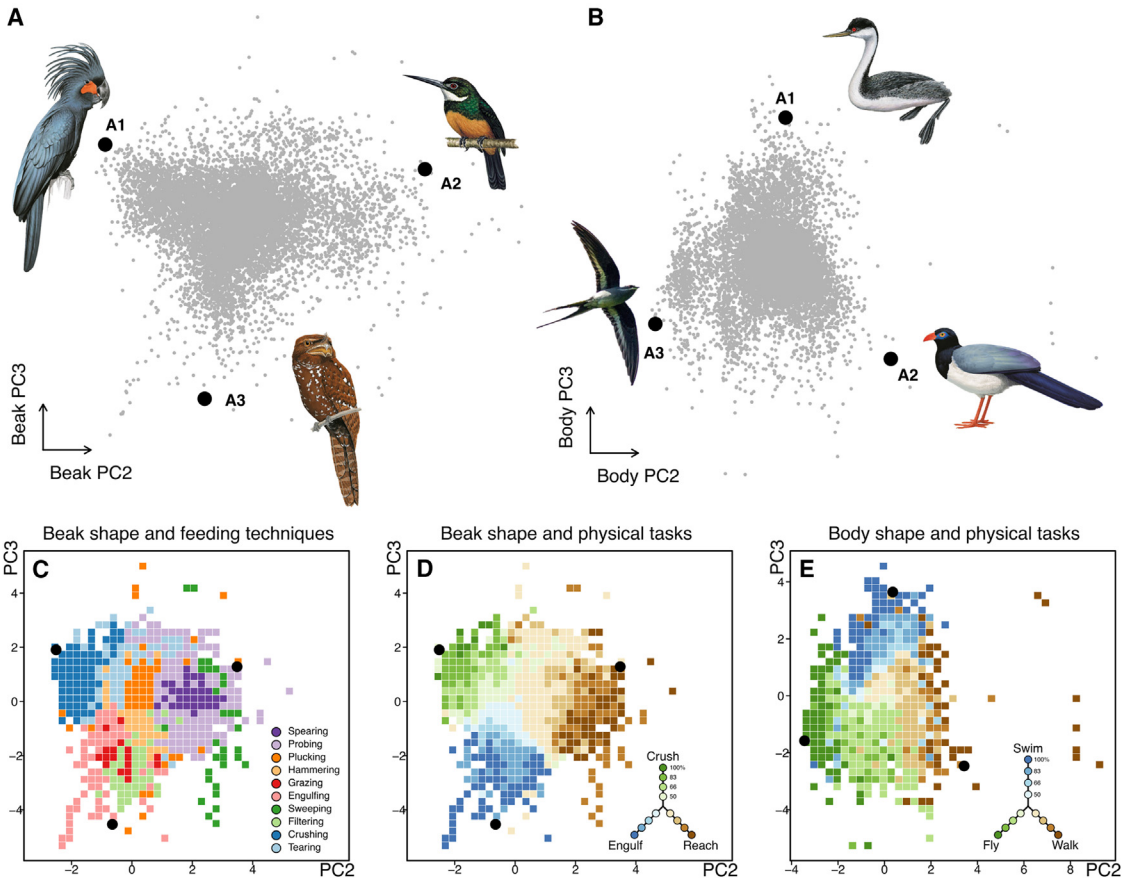

Figure 2. Trade-offs constrain beak and body shape variation to simple triangles

(A) Beak principal component (PC) 2 and 3 describe variation in relative beak length (PC2) and relative width and depth (PC3).

(B) Body PC2 and PC3 describe variation in relative length of the legs versus wings (PC2) and the tail (PC3). Gray points show the distribution of individual species in morphospace for beak shape (n = 9,942) and body shape (n = 9,926). Black circles show the position of "archetypes" (i.e., vertices) defining the best-fitting triangle for describing beak and body shape variation.

(C) Primary feeding techniques mapped across beak morphospace.

(D) Primary physical tasks mapped across beak morphospace.

(E) Primary physical tasks mapped across body morphospace.

The color and shade of occupied cells in lower panels indicate relative prevalence of physical tasks. In (D) and (E), the names of archetypal tasks follow definitions in Table 1. Examples of species close to archetypal positions are included with permission from Lynx Nature Books and Cornell Lab of Ornithology (see acknowledgments).

See Figures S2–S6 and Tables S1 and S2.

rather than restrictions on extreme trait combinations per se, appear to be the primary way in which observed variation in beak form is constrained below what is geometrically possible.

A principal-component analysis (PCA) indicates that the main dimension of beak form variation represents differences in size, with PC1 capturing 86% of the variance in beak dimensions (Table S1). Beak size varies by >5 orders of magnitude across species—from the Antillean palm swift *Tachornis phoenicobia* to the Shoebill *Balaeniceps rex*—likely reflecting the enormous variation in the size of exploited food items,[2,31] as well as additional selective pressures, such as thermoregulation.[38,39] Each trait has an almost equivalent loading on PC1, indicating that beak shape is largely invariant with size (Table S1) so that the most massive beaks are essentially scaled-up versions of the smallest beaks (Figure 1A). Given the observed bounds of each beak trait, bird beaks have evolved to occupy almost the full range (84%) of geometrically possible sizes, from the most massive to the most miniature (Figure S1B). Taken together, these results reveal how the restricted volume of beak morphospace largely reflects a high co-variation among beak traits that results in a lack of extreme shapes rather than simply restrictions on size. To examine constraints on the beak independent of size, we focused the rest of our analyses on the variation in the second and third dimensions of beak principal component (PC) space, which describe the relative length (PC2) and relative width and depth (PC3) of the beak, respectively.

Geometry of beak shape variation

Rather than occupying an amorphous region across the 2D plane defined by PC2 and PC3, beak shape morphospace resembles a triangle, with diffuse but relatively clearly defined edges and vertices (Figure 2A). Morphospaces conforming to

Please cite this article in press as: Sayol et al., Ecophysical constraints on avian adaptation and diversification, Current Biology (2025), https://doi.org/10.1016/j.cub.2025.02.015

simple geometrical patterns, like lines, triangles, or trapezoids, are predicted by optimization theory when there are trade-offs to performing a limited number of tasks.[17,40] According to this theory, performance of a given task is optimized at a single point in morphospace and declines away from this "archetype." When selection acts on the performance of two tasks, trade-offs will cause species traits to be organized along the line connecting the two archetypes. This region where performance is maximized is termed the Pareto front. With trade-offs among three tasks, the Pareto front expands to occupy a triangular region of morphospace, with each vertex of the triangle corresponding to realized or theoretical trait combinations that are specialized to perform one of the three tasks.[17] With a large number of tasks, morphospace would increasingly resemble a circle. Thus, according to this theory, the number of vertices defining morphospace is indicative of the number of trade-offs shaping morphological diversity.

To formally test how well beak shape morphospace conforms to a triangle, we fitted to the boundaries of the empirical point cloud a series of polygons, varying both the number and location of vertices. When polygons are allowed to take irregular shapes, adding more vertices (i.e., archetypes) will always improve fit. However, we found that the improvement in fit beyond three vertices is marginal (Figure S2). For regular polygons, adding more than three vertices results in a poorer fit (Figure S3), confirming the visual impression that beak shape morphospace can be well described by a triangle. This triangular pattern is not an artifact of the simple linear measurements we used to characterize beak morphospace because we recovered the same triangular geometry when using the two primary shape axes derived from 3D beak scans available for a subset of species (Figure S4A). A triangular pattern is also robust to including PC1 (i.e., beak size) and modeling the position of archetypes in 3D beak morphospace, indicating that the morphological form of archetypes is replicated across species with small and large beaks (Figure S5A). While PCA on skewed trait distributions can generate apparently triangular shapes, null model simulations using a randomized set of the real trait values show that skewness alone is unlikely to explain the triangular shape of the avian morphospace ($p < 0.05$; Table S2, randomized (RND) null model). Simulations of trait evolution assuming a Brownian motion (BM) model also show that morphospaces with few vertices cannot be explained simply by the unbalanced shape of the avian phylogeny ($p < 0.05$; Table S2, BM null model).

The first archetype (A1) of beak shape morphospace describes beaks that are short, narrow, and deep (Figure 2A). The second archetype (A2) describes beaks that are long relative to their width and depth. The third archetype (A3) describes beaks that are of intermediate length, flat, and wide. A possible fourth archetype (Figure S2D) corresponds to long, deep, and laterally flattened beaks such as those of Skimmers (genus *Rynchops*) and Puffins (genus *Fratercula*). These aquatic species have knife-like or hatchet-like beaks apparently designed for slicing through water and, in the latter case, digging soil. However, this vertex is shallow, weakly supported, and potentially reflects curvature in the edge of morphospace, between archetypes A1 and A2. Such curved edges connecting archetypes are not unexpected under the Pareto front concept and can arise if the performance of a task is optimized across a region rather than at a particular point in morphospace or if changes in performance of a given task do not occur uniformly across morphospace.[18] While the restricted volume and geometry of beak morphospace are consistent with the idea that trade-offs among a small number of tasks have constrained the variety of beak forms, a stronger test requires identifying these tasks and how they are distributed across beak morphospace.

Tradeoffs constraining beak form and function

Bird beaks are used in multiple ecological contexts, including nest building[41] and thermoregulation,[38,39] but their most essential role is the acquisition and processing of resources.[2,42] We hypothesize that the triangular shape of beak morphospace represents trade-offs between three extreme physical tasks—to crush, reach, or engulf food. All beaks require resistance to structural stress (i.e., yield strength) to avoid fracturing, but this requirement is particularly acute for species crushing hard food items (e.g., seeds). A crushing action requires resistance to bending in the dorsoventral direction, which, for a given beak size, can be achieved by a relative deepening of the beak (i.e., low PC2 and high PC3).[14,43] This beak geometry corresponds to archetype 1 in the top left region of beak shape morphospace. However, a relatively deeper beak comes at the expense of a slower closing velocity and a reduction in the efficiency of prey acquisition,[44] which should be maximized by either a relative widening (i.e., lower PC3) or elongation (i.e., higher PC2) of the beak to either engulf or reach food. All else being equal, extreme widening of the beak (archetype 3) maximizes the open-mouth surface area, which tends to increase the quantity of plant material harvested during grazing,[45] the volume of water that can be filtered for food,[46] or the ability to capture prey in flight.[47] By contrast, extreme elongation of the beak (archetype 2) provides a longer closing surface and sweeping circle for capturing fast-moving prey,[42,48] as well as a probing device for accessing animals concealed in a variety of crevices or buried in soft sediments, or the nectar within flowers. Crucially, for a given beak size, increases in the capacity to crush, engulf, or reach food are expected to come at the expense of performing the other physical tasks.

We currently lack experimental data on task performance at global scales, so instead we provide a coarse-level assessment of how these tasks map onto beak morphospace using information on ten feeding behaviors describing the techniques used by species to obtain and process these resources (Tables 1 and S3). For each feeding technique (Figure 2C), we developed a heuristic scoring system that, although highly simplified, aims to capture the relative reliance on each physical task (Table S3). For example, probing for nectar relies on a long reach but no capacity to crush or engulf, so it would receive a score of 1, 0, and 0 for these tasks, respectively. Other cases are more challenging to score. For example, behaviors involving hammering or tearing require resistance to bending stress during impact and torsional loading, respectively. While distinct from the task of crushing, these feeding techniques share the same requirement for a high yield strength, and so to reflect this, they would also receive positive scores for the crush task. Despite these challenges, we found that the three beak physical tasks map out with remarkable fidelity to the three vertices of beak morphospace in a way that matches expectations (Figure 2D). At each vertex, species are specialized at using a single physical task, with the specialization on that task

Please cite this article in press as: Sayol et al., Ecophysical constraints on avian adaptation and diversification, Current Biology (2025), https://doi.org/10.1016/j.cub.2025.02.015

Table 1. Summary of ecological variables

Concept	Definition
Feeding technique	specific method or behavior employed by a bird to acquire and process food using its beak. In our study, we distinguish 10 feeding techniques: tearing, crushing, engulfing, filtering, sweeping, grazing, hammering, plucking, probing, and spearing (see definitions in Table S3).
Foraging niche	specific ecological role that a species occupies, combining both the foraging behavior used by birds to search for or capture their preferred food sources within their respective habitats and the type of food eaten. In our study, we distinguish 32 foraging niches, e.g., "Frugivore ground" or "Invertivore aerial screening" (see definitions in Table S4).
Physical task	primary goals or tasks that a certain phenotype is adapted to achieve in relation to feeding or foraging. We define three main physical tasks for beak shape (crush, reach, and engulf) and three physical tasks for body shape here corresponding to efficient movement through (or over) the three different states of matter (fly, walk, and swim). The scores for mapping feeding techniques and foraging niches to each physical task are included in Tables S3 and S4. The names applied to archetypal tasks are simplified for clarity. For example, bird beaks are designed to crush, reach, or engulf, with crush being a catch-all term for tasks requiring strong bite force, such as cutting or tearing.

Definitions of the different types of ecological variables related to food acquisition and locomotion used in the study. See Tables S3 and S4 for full definitions.

then declining away from that vertex (Figures 2D and 3A–3C). Species positioned away from the vertices, either along the boundaries or in the center of morphospace, feed in ways that require balancing the capacity for two and three different physical tasks, respectively. These findings were robust to varying the precise way we scored physical tasks for each feeding technique (Figures S6A–S6C). The distribution of ecophysical specialists and generalists in morphospace is consistent with the idea that trade-offs among a small number of primary physical tasks constrain the set of realized beak forms across the avian radiation. Further studies are required to corroborate this evidence using more highly refined quantitative data, including estimates of functional performance and additional axes of beak shape variation (e.g., curvature).[31]

Ecophysical constraints on body morphospace

The beak is the principal apparatus used by birds for acquiring and processing resources, yet it only provides an incomplete description of the trophic niche. For example, species with similarly shaped beaks can use substantially different foraging strategies, each describing how organisms move through the environment to locate and procure their food (Table 1). To address this, we extended our analysis to consider constraints on variation in body shape using a PCA of the key traits linked to locomotion in birds: the wing, tail, and tarsus (Table S1). We found that the same patterns of constraint identified for beak shape also apply to body shape. Specifically, body shape morphospace defined by PC2 and PC3 is well described by a polygon with three vertices (Figure 2B; see body shape in Figures S2 and S3). We hypothesized that this triangular shape reflects constraints on movement imposed by the three primary physical states of matter inhabited or exploited by species: air, water, and solid substrates.[49–51] For the purpose of simplified models, we broadly characterize these imperatives as the capacity to fly, swim, or walk, while recognizing that each of these physical tasks belies a diversity of finer-grained behavioral variation (e.g., walking, running, hopping, and climbing are here treated simply as variants of the capacity to walk).

To examine this hypothesis in our ecomorphological framework, we mapped the distribution of physical tasks across body morphospace using data on species foraging niches that describe diet, habitat use, and behavior (Tables 1 and S4), scoring these according to their reliance on each of the three body physical tasks. We find that the three vertices of the Pareto front correspond to body forms specialized to swim (A1), walk (A2), or fly (A3), with intermediate forms being more generally associated with multiple physical media (Figures 2E and 3D–3F). Thus, similarly to beak shape, our results suggest that the primary axes of variation in body shape are also constrained by trade-offs among a small number of physical tasks, in this case related to three locomotory modalities.

Evolutionary dynamics of a bounded morphospace

The bounded nature of bird beak and body morphospace inferred by our analysis helps explain several macroevolutionary trends. The evolution of beak shape among extant birds is characterized by an early expansion of disparity, while over the last ~50 million years the volume of beak morphospace has remained relatively stable, despite rapid and ongoing species evolution.[31] During this latter period of morphospace infilling, evolutionary convergence has been pervasive, with distantly related bird lineages repeatedly converging on the same regions of beak and body morphospace.[2,52] The constraints on morphospace that we identify could explain both the stalling of beak disparification and the widespread evolutionary convergence in morphology, as divergence into novel regions of morphospace is limited.

To explore how bird morphospace has filled over time, we performed a phylogenetic reconstruction of beak and body shape, analyzing the flux of phenotypic evolution across morphospace by comparing the morphological position of descendant and ancestor nodes. Allowing for variation in rates of evolution across lineages and over time, we inferred a net outward flow of lineages from the densely packed core to the periphery and corners of the Pareto front: 63.7% of lineages for beak (Figure 4A) and 64% for body shape (Figure 4B). This pattern could be expected

Please cite this article in press as: Sayol et al., Ecophysical constraints on avian adaptation and diversification, Current Biology (2025), https://doi.org/10.1016/j.cub.2025.02.015

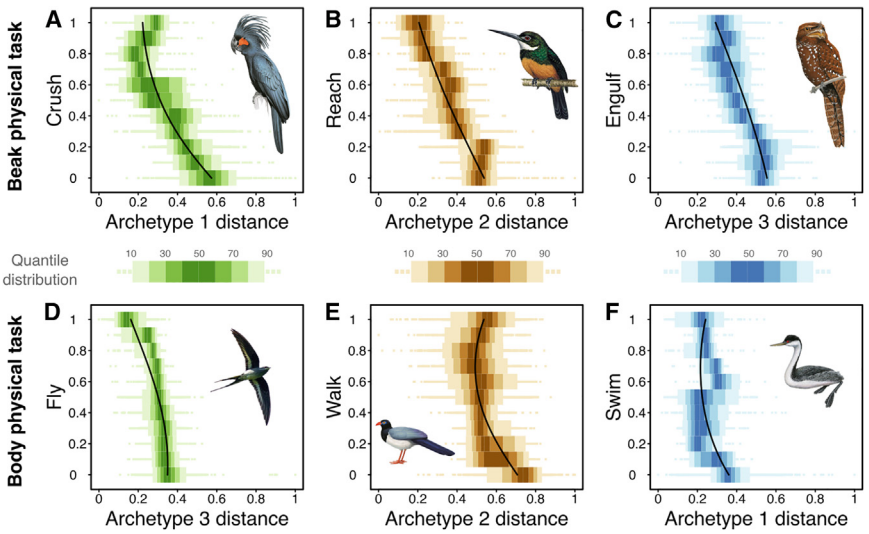

Figure 3. Specialization on each physical task as a function of the distance the corresponding archetype (vertex)

Results are shown for beak (A–C) and body (D–F) shape morphospace (n = 9,942 and n = 9,926 species, respectively). In all panels, the y axis shows specialization as the proportional use of each particular physical task. For each level of specialization, horizontal box plots show the distribution of distances from the focal archetype (the shading of color bands within boxes delimit 10% quantiles). Fitted lines are from a quadratic beta-regression predicting distance as a function of specialization on the respective task. Distances to archetypes were rescaled between 0.01 and 0.99 for model fitting and plotting. Examples of species close to archetypal positions are included with permission from Lynx Nature Books and Cornell Lab of Ornithology (see acknowledgments). See also Figure S6.

simply for geometric reasons[53] (see STAR Methods), so we compared our reconstructions to those expected under a null variable rate model of Brownian trait evolution. We found that lineages were more likely to evolve outward to the vertices of beak and body shape morphospace than expected by chance. For beak shape, this non-random trend was evident both globally (null model: 95% CI 54.7%–60.9%, $p_{null} < 0.01$) and within localized regions of beak morphospace (i.e., local directionality tested within grid cells covering morphospace, see STAR Methods). For body shape, the null model of random evolution could not be rejected at a global scale (null model 95% CI 62.1%–65.0%, $p_{null} < 0.33$), but within those localized regions of body shape morphospace where the null model could be rejected, an average outward trajectory was far more common (87% of cases of arrows moving outward in Figure 4B) than an average inward (13% of arrows) trajectory. Together, these results support the hypothesis that, despite much heterogeneity, lineages tend to evolve greater specialization on singular physical tasks over macroevolutionary time.[54,55] These inferences should be interpreted with caution given the coarse nature of the data and the known challenges of inferring long-extinct ancestral forms.[56] Besides, a potential net outward flow of lineages does not explain the bounded structure of morphospace, nor the greater concentration of species in its core compared with the edges of the Pareto front.[2,36,57]

One possible explanation for the relative scarcity of species near and beyond the boundaries of the Pareto front might be a higher risk of extinction of functionally specialized species,[33–36] lower rates of speciation, or both.[37] Mapping the incidence of currently threatened species and of lineages with historically fast speciation rates reveals extinction (Figures 4C and 4D) and speciation (Figures 4E and 4F) hotspots across beak and body morphospace. These hotspots of high extinction risk and speciation rate tend to cluster around the edges and often near the corners of the Pareto front (i.e., archetypes) where functional specialization is highest. The possibility of peripheral hotspots of extinction and speciation is intriguing because it suggests a dynamic of greater macroevolutionary turnover of lineages at the edge of the Pareto front, which could accelerate the creation of new ecological opportunities, thereby driving the net outward flow of lineages from the core, while also capping the density of species at the edge (Figures 4A and 4B).

Further research is needed to evaluate this possibility, as the patterns detected in our analyses are noisy and inconclusive. Some peripheral regions of morphospace are not consistently associated with increased extinction (e.g., body A3) or speciation (e.g., body A1) (Figures 4D and 4F). In addition, in species-level models accounting for phylogenetic non-independence and other potential confounding variables, we found that there was no consistent effect of distance to archetypes on speciation rates, with extinction risk only significantly increasing toward body and not beak archetypes (Table S5). Thus, while the distribution of current threat across morphospace is in line with the notion that specialized species are more sensitive to anthropogenic environmental change,[58,59] our global analysis suggests that physical specialization may not consistently predict rates of speciation or extinction.

A potential explanation for the inconsistency of these findings is that a focus on current patterns of threat and recent rates of speciation may fail to capture the macroevolutionary dynamics that have shaped morphospace throughout avian history.[60,61] Future work could focus on incorporating data from prehistoric extinctions[62] to evaluate if species beyond the edge of the Pareto front indeed experience higher turnover. Alternatively, if the lack of a general link between diversification dynamics and physical specialization does also operate over deep macroevolutionary time, this would suggest that the triangular boundary of avian beak and body morphospace is not maintained by selection at or above the species level,[63] but instead reflects microevolutionary processes, with constraints on adaptation inhibiting the evolution of more extreme trait combinations. The edges to morphospace that these constraints impose need not correspond to "hard" boundaries beyond which trait combinations are physically impossible.[9,10] After all, the peripheral regions of trait space beyond the Pareto front are sparsely filled but not completely empty, containing ecomorphological oddities such

Please cite this article in press as: Sayol et al., Ecophysical constraints on avian adaptation and diversification, Current Biology (2025), https://doi.org/10.1016/j.cub.2025.02.015

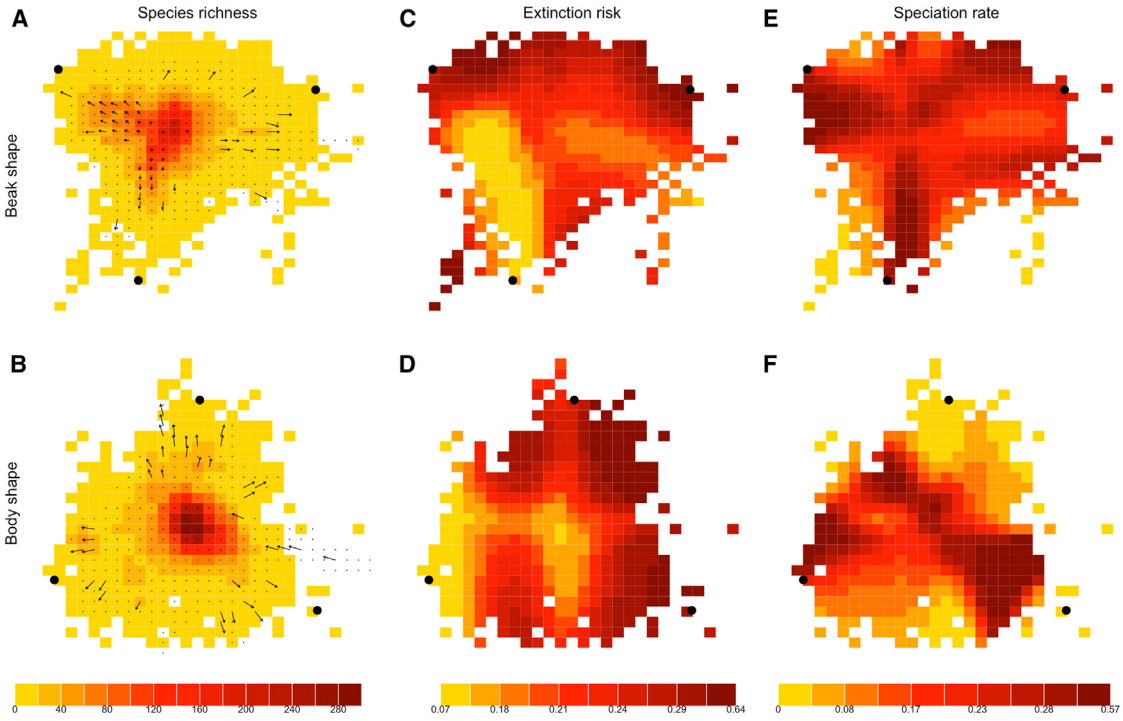

Figure 4. Macroevolutionary dynamics of beak and body shape morphospace

(A and B) Species richness and the mean direction of trait evolution (arrows) mapped across beak and body shape morphospace. Predicted probability of a species being threatened with extinction (C and D) and being in the top speciation rate quartile (E and F) mapped across beak and body morphospace. Archetypes defining the triangular Pareto front are indicated as black points. In (A and B), arrows show the mean direction of evolution along the branches reconstructed to intersect each grid cell. Longer vectors indicate a greater consistency in direction (i.e., a lower variance). Arrows are replaced with points if the consistency in the direction of evolution was no greater than expected under a model of random trait diffusion.

See also Figure S7 and Table S5.

as Horned Puffin (*Fratercula corniculata*), Royal Spoonbill (*Platalea regia*), and Indian Skimmer (*Rynchops albicollis*) for beak shape and Lyre-tailed nightjar (*Uropsalis lyra*), Böhm's Spinetail (*Neafrapus boehmi*), and the Emu (*Dromaius novaehollandiae*) for body shape. Instead, we suggest that trade-offs constrain most species to occur within the triangular Pareto front,[17,18] while the relaxation of selection due to key innovations or geographical isolation from competitors[64,65] allows some lineages to persist beyond the Pareto front. In any case, release from these selective constraints appears to be sufficiently rare or fleeting to maintain the overall triangular structure of morphospace.

Functional specialization and the limits of morphological evolution

While trade-offs among a limited number of physical tasks appear to constrain the shape of avian morphospace, ecological limits to coexistence could cause variation in species density within these bounds. The central core of high species density (Figures 4A and 4B) is largely composed of predators that glean invertebrates from plant surfaces (Figures S7A and S7B) for which the structural complexity of the habitat and the enormous diversity of prey items could lead to a finer partitioning of ecological niches, thus enhancing species coexistence.[42,66,67] Our data support this explanation, showing that species near the center of morphospace have narrower foraging niches, consistent with the compression of niche breadth linked to high species packing (Figures S7A and S7B). Our results further show that this ecological niche specialization does not correspond to physical specialization and that arboreal gleaning invertivores—which comprise by far the most diverse foraging niche—are actually generalists in their physical tasks (Figures S7C and S7D). In effect, their beak shapes reflect a trade-off between crushing, reaching, and engulfing prey, and their body shapes a trade-off between frequent flight and perching (i.e., a combination of flying and terrestrial locomotion).

The morphology of birds—with their feathered wings and keratinous beaks—is unique in the animal kingdom, occupying only a small subset of the enormous morphological variety of heterotrophic organisms. The limits to avian evolution inferred by our analysis would thus reflect the ecophysical constraints operating in the context of the developmental pathways and body plan of birds. Yet, these trade-offs would also seem sufficiently fundamental to suggest a general framework for organizing this wider animal diversity. For evolutionary radiations spanning multiple physical realms, our findings predict that the primary axes of body shape variation should conform to lines, triangles, or perhaps quadrilaterals, according to the number of physical states of matter through or upon which organisms move.[68,69] Similarly, the fundamental trade-off of whether to crush, reach, and engulf food that constrains beak evolution to a triangular Pareto front could apply to the skulls of other vertebrates that

also primarily catch and process resources using their mouths.[48,70] The deep beak of a cockatoo (A1; Figure 2A) cracking the hard kernel of a seed resembles in its function the robust skull of a bone-crunching hyena.[71] A butterfly plucked in mid-flight by the forceps-like beak of a jacamar (A2; Figure 2A) meets the same fate as a fish snatched by the elongated jaws of a gharial,[48] and the wide gape of a frogmouth engulfing its soft-bodied prey (Figure 2A; A3) draws parallels with a baleen whale hunting with its huge jaws agape.[46] While the diversity of body plans and the lack of quantitative morphological data have previously hindered efforts to integrate and combine morphospaces spanning multiple animal classes, the identification of universal ecophysical constraints can allow us to orientate and position species across these trade-offs, moving us closer to a general and mechanistic understanding of the origins, maintenance, and functioning of animal biodiversity and how this responds to environmental change.

RESOURCE AVAILABILITY

Lead contact

Further information and requests should be directed to and will be fulfilled by the lead contact, Ferran Sayol (fsayol@gmail.com).

Materials availability

This study did not generate new unique reagents.

Data and code availability

- Data generated for this study are available at https://github.com/fsayol/BirdArchetypes.
- Code to run the analysis is available at https://github.com/fsayol/BirdArchetypes.
- Any additional information required to reanalyze the data reported in this paper is available from the lead contact upon request.

ACKNOWLEDGMENTS

We thank the many researchers, volunteers, and institutions who contributed to the AVONET dataset used in this study. F.S. was funded by the European Union's Horizon 2020 research and innovation program under the Marie Skłodowska-Curie grant agreement no. 838998 and by "la Caixa" foundation (ID 100010434) through a Junior Leader program (LCF/BQ/PI23/11970019). A.L.P. was supported by a Royal Society University Research fellowship. The credits for species images used in Figures 2 and 3 are as follows: *Prosciger aterrimus* by Ian Lewington, *Brachygalba salmoni* by Clive Byers, *Rigidipenna inexpectata* by Tim Worfolk, *Carpococcyx renauldi* by Chris Rose, *Aechmophorus occidentalis* by Lluís Solé, and *Hemiprocne mystacea* by Benjamin van Doren.

AUTHOR CONTRIBUTIONS

F.S., J.A.T., and A.L.P. developed the conceptual framework and designed the study. F.S., A.L.P., and B.R.R. compiled and analyzed data with support from J.A.T. F.S., J.A.T., and A.L.P. wrote the manuscript with support from B.R.R.

DECLARATION OF INTERESTS

The authors declare no competing interests.

STAR★METHODS

Detailed methods are provided in the online version of this paper and include the following:

SUPPLEMENTAL INFORMATION

Supplemental information can be found online at https://doi.org/10.1016/j.cub.2025.02.015.

Received: March 16, 2024
Revised: October 26, 2024
Accepted: February 7, 2025
Published: March 4, 2025

REFERENCES

1. Díaz, S., Kattge, J., Cornelissen, J.H.C., Wright, I.J., Lavorel, S., Dray, S., Reu, B., Kleyer, M., Wirth, C., Prentice, I.C., et al. (2016). The global spectrum of plant form and function. Nature *529*, 167–171. https://doi.org/10.1038/nature16489.
2. Pigot, A.L., Sheard, C., Miller, E.T., Bregman, T.P., Freeman, B.G., Roll, U., Seddon, N., Trisos, C.H., Weeks, B.C., and Tobias, J.A. (2020). Macroevolutionary convergence connects morphological form to ecological function in birds. Nat. Ecol. Evol. *4*, 230–239. https://doi.org/10.1038/s41559-019-1070-4.
3. Price, S.A., Friedman, S.T., Corn, K.A., Martinez, C.M., Larouche, O., and Wainwright, P.C. (2019). Building a body shape morphospace of teleostean fishes. Integr. Comp. Biol. *59*, 716–730. https://doi.org/10.1093/icb/icz115.
4. Schluter, D. (2000). The Ecology of Adaptive Radiation (Oxford University Press).
5. Title, P.O., Singhal, S., Grundler, M.C., Costa, G.C., Pyron, R.A., Colston, T.J., Grundler, M.R., Prates, I., Stepanova, N., Jones, M.E.H., et al. (2024). The macroevolutionary singularity of snakes. Science *383*, 918–923.
6. Raup, D.M. (1966). Geometric analysis of shell coiling: general problems. J. Paleontol. 1178–1190.
7. Garland, T., Jr., Downs, C.J., and Ives, A.R. (2022). Trade-offs (and constraints) in organismal biology. Physiol. Biochem. Zool. *95*, 82–112.
8. Arnold, S.J. (1992). Constraints on phenotypic evolution. Am. Nat. *140*, S85–S107.
9. Alexander, R.M. (1985). The ideal and the feasible: physical constraints on evolution. Biol. J. Linn. Soc. *26*, 345–358.
10. Kempes, C.P., Koehl, M.A.R., and West, G.B. (2019). The scales that limit: the physical boundaries of evolution. Front. Ecol. Evol. *7*, 242.
11. Higham, T.E., Ferry, L.A., Schmitz, L., Irschick, D.J., Starko, S., Anderson, P.S.L., Bergmann, P.J., Jamniczky, H.A., Monteiro, L.R., Navon, D., et al. (2021). Linking ecomechanical models and functional traits to understand phenotypic diversity. Trends Ecol. Evol. *36*, 860–873. https://doi.org/10.1016/j.tree.2021.05.009.
12. Taylor, G., and Thomas, A. (2014). Evolutionary Biomechanics: Selection, Phylogeny, and Constraint (Oxford University Press).
13. Arnold, S.J. (1983). Morphology, performance and fitness. Am. Zool. *23*, 347–361.

14. Deakin, W.J., Anderson, P.S.L., den Boer, W., Smith, T.J., Hill, J.J., Rücklin, M., Donoghue, P.C.J., and Rayfield, E.J. (2022). Increasing morphological disparity and decreasing optimality for jaw speed and strength during the radiation of jawed vertebrates. Sci. Adv. *8*, eabl3644. https://doi.org/10.1126/sciadv.abl3644.

15. Gallagher, A.J., Hammerschlag, N., Cooke, S.J., Costa, D.P., and Irschick, D.J. (2015). Evolutionary theory as a tool for predicting extinction risk. Trends Ecol. Evol. *30*, 61–65.

16. Ryding, S., Klaassen, M., Tattersall, G.J., Gardner, J.L., and Symonds, M.R.E. (2021). Shape-shifting: changing animal morphologies as a response to climatic warming. Trends Ecol. Evol. *36*, 1036–1048. https://doi.org/10.1016/j.tree.2021.07.006.

17. Shoval, O., Sheftel, H., Shinar, G., Hart, Y., Ramote, O., Mayo, A., Dekel, E., Kavanagh, K., and Alon, U. (2012). Evolutionary trade-offs, Pareto optimality, and the geometry of phenotype space. Science *336*, 1157–1160. https://doi.org/10.1126/science.1217405.

18. Sheftel, H., Shoval, O., Mayo, A., and Alon, U. (2013). The geometry of the Pareto front in biological phenotype space. Ecol. Evol. *3*, 1471–1483. https://doi.org/10.1002/ece3.528.

19. MacArthur, R.H. (1984). Geographical Ecology: Patterns in the Distribution of Species (Princeton University Press).

20. West, G.B., Brown, J.H., and Enquist, B.J. (1997). A general model for the origin of allometric scaling laws in biology. Science *276*, 122–126. https://doi.org/10.1126/science.276.5309.122.

21. Haldane, J.B. (1926). On being the right size. Harpers Mag. *152*, 424–427.

22. Puglielli, G., Hutchings, M.J., and Laanisto, L. (2021). The triangular space of abiotic stress tolerance in woody species: a unified trade-off model. New Phytol. *229*, 1354–1362. https://doi.org/10.1111/nph.16952.

23. Pavanetto, N., Carmona, C.P., Laanisto, L., Niinemets, Ü., and Puglielli, G. (2024). Trait dimensions of abiotic stress tolerance in woody plants of the Northern Hemisphere. Global Ecol. Biogeogr. *33*, 272–285. https://doi.org/10.1111/geb.13788.

24. Chave, J., Coomes, D., Jansen, S., Lewis, S.L., Swenson, N.G., and Zanne, A.E. (2009). Towards a worldwide wood economics spectrum. Ecol. Lett. *12*, 351–366. https://doi.org/10.1111/j.1461-0248.2009.01285.x.

25. Wright, I.J., Reich, P.B., Westoby, M., Ackerly, D.D., Baruch, Z., Bongers, F., Cavender-Bares, J., Chapin, T., Cornelissen, J.H.C., Diemer, M., et al. (2004). The worldwide leaf economics spectrum. Nature *428*, 821–827. https://doi.org/10.1038/nature02403.

26. Rogers, H.S., Donoso, I., Traveset, A., and Fricke, E.C. (2021). Cascading Impacts of Seed Disperser Loss on Plant Communities and Ecosystems. Annu. Rev. Ecol. Evol. Syst. *52*, 641–666. https://doi.org/10.1146/annurev-ecolsys-012221-111742.

27. Butterfield, N.J. (2011). Animals and the invention of the Phanerozoic Earth system. Trends Ecol. Evol. *26*, 81–87.

28. Tobias, J.A., Sheard, C., Pigot, A.L., Devenish, A.J.M., Yang, J., Sayol, F., Neate-Clegg, M.H.C., Alioravainen, N., Weeks, T.L., Barber, R.A., et al. (2022). AVONET: morphological, ecological and geographical data for all birds. Ecol. Lett. *25*, 581–597. https://doi.org/10.1111/ele.13898.

29. Grant, P.R. (1999). Ecology and Evolution of Darwin's Finches (Princeton University Press).

30. Jønsson, K.A., Fabre, P.-H., Fritz, S.A., Etienne, R.S., Ricklefs, R.E., Jørgensen, T.B., Fjeldså, J., Rahbek, C., Ericson, P.G.P., Woog, F., et al. (2012). Ecological and evolutionary determinants for the adaptive radiation of the Madagascan vangas. Proc. Natl. Acad. Sci. USA *109*, 6620–6625.

31. Cooney, C.R., Bright, J.A., Capp, E.J.R., Chira, A.M., Hughes, E.C., Moody, C.J.A., Nouri, L.O., Varley, Z.K., and Thomas, G.H. (2017). Mega-evolutionary dynamics of the adaptive radiation of birds. Nature *542*, 344–347. https://doi.org/10.1038/nature21074.

32. Irschick, D.J., and Higham, T.E. (2016). Animal Athletes: an Ecological and Evolutionary Approach (Oxford University Press).

33. Davies, K.F., Margules, C.R., and Lawrence, J.F. (2004). A synergistic effect puts rare, specialized species at greater risk of extinction. Ecology *85*, 265–271. https://doi.org/10.1890/03-0110.

34. Sayol, F., Cooke, R.S.C., Pigot, A.L., Blackburn, T.M., Tobias, J.A., Steinbauer, M.J., Antonelli, A., and Faurby, S. (2021). Loss of functional diversity through anthropogenic extinctions of island birds is not offset by biotic invasions. Sci. Adv. *7*, eabj5790. https://doi.org/10.1126/sciadv.abj5790.

35. Ali, J.R., Blonder, B.W., Pigot, A.L., and Tobias, J.A. (2023). Bird extinctions threaten to cause disproportionate reductions of functional diversity and uniqueness. Funct. Ecol. *37*, 162–175. https://doi.org/10.1111/1365-2435.14201.

36. Hughes, E.C., Edwards, D.P., and Thomas, G.H. (2022). The homogenization of avian morphological and phylogenetic diversity under the global extinction crisis. Curr. Biol. *32*, 3830–3837.e3. https://doi.org/10.1016/j.cub.2022.06.018.

37. Futuyma, D.J. (2010). Evolutionary constraint and ecological consequences. Evolution *64*, 1865–1884. https://doi.org/10.1111/j.1558-5646.2010.00960.x.

38. Tattersall, G.J., Andrade, D.V., and Abe, A.S. (2009). Heat exchange from the toucan bill reveals a controllable vascular thermal radiator. Science *325*, 468–470. https://doi.org/10.1126/science.1175553.

39. Greenberg, R., Cadena, V., Danner, R.M., and Tattersall, G.J. (2012). Heat loss may explain bill size differences between birds occupying different habitats. PLoS ONE *7*, e40933. https://doi.org/10.1371/journal.pone.0040933.

40. Hart, Y., Sheftel, H., Hausser, J., Szekely, P., Ben-Moshe, N.B., Korem, Y., Tendler, A., Mayo, A.E., and Alon, U. (2015). Inferring biological tasks using Pareto analysis of high-dimensional data. Nat. Methods *12*, 233–235. https://doi.org/10.1038/nmeth.3254.

41. Sheard, C., Street, S.E., Evans, C., Lala, K.N., Healy, S.D., and Sugasawa, S. (2023). Beak shape and nest material use in birds. Philos. Trans. R. Soc. Lond. B Biol. Sci. *378*, 20220147. https://doi.org/10.1098/rstb.2022.0147.

42. Navalón, G., Bright, J.A., Marugán-Lobón, J., and Rayfield, E.J. (2019). The evolutionary relationship among beak shape, mechanical advantage, and feeding ecology in modern birds. Evolution *73*, 422–435. https://doi.org/10.1111/evo.13655.

43. Dickinson, E., Young, M.W., and Granatosky, M.C. (2022). *In vivo* bite force in lovebirds (*Agapornis roseicollis*, Psittaciformes) and their relative biting performance among birds. J. Zool. *318*, 272–282. https://doi.org/10.1111/jzo.13014.

44. Corbin, C.E., Lowenberger, L.K., and Gray, B.L. (2015). Linkage and trade-off in trophic morphology and behavioural performance of birds. Funct. Ecol. *29*, 808–815. https://doi.org/10.1111/1365-2435.12385.

45. Arsenault, R., and Owen-Smith, N. (2008). Resource partitioning by grass height among grazing ungulates does not follow body size relation. Oikos *117*, 1711–1717.

46. Field, D.J., Lin, S.C., Ben-Zvi, M., Goldbogen, J.A., and Shadwick, R.E. (2011). Convergent evolution driven by similar Feeding mechanics in Balaenopterid whales and pelicans. Anat. Rec. (Hoboken) *294*, 1273–1282. https://doi.org/10.1002/ar.21406.

47. Jones, L.R., Black, H.L., and White, C.M. (2012). Evidence for convergent evolution in gape morphology of the bat hawk (*Macheiramphus alcinus*) with swifts, swallows, and goatsuckers. Biotropica *44*, 386–393. https://doi.org/10.1111/j.1744-7429.2011.00812.x.

48. McCurry, M.R., Walmsley, C.W., Fitzgerald, E.M.G., and McHenry, C.R. (2017). The biomechanical consequences of longirostry in crocodilians and odontocetes. J. Biomech. *56*, 61–70.

49. Zeffer, A., Johansson, L.C., and Marmebro, Å. (2003). Functional correlation between habitat use and leg morphology in birds (Aves). Biol. J. Linn. Soc. *79*, 461–484. https://doi.org/10.1046/j.1095-8312.2003.00200.x.

50. Tobalske, B.W. (2007). Biomechanics of bird flight. J. Exp. Biol. *210*, 3135–3146. https://doi.org/10.1242/jeb.000273.

51. Heers, A.M., and Dial, K.P. (2015). Wings versus legs in the avian *bauplan*: Development and evolution of alternative locomotor strategies. Evolution *69*, 305–320. https://doi.org/10.1111/evo.12576.

52. Ksepka, D.T., Grande, L., and Mayr, G. (2019). Oldest finch-beaked birds reveal parallel ecological radiations in the earliest evolution of Passerines. Curr. Biol. *29*, 657–663.e1. https://doi.org/10.1016/j.cub.2018.12.040.

53. Fisher, R.A. (1930). The Genetical Theory of Natural Selection (The Clarendon Press).

54. Futuyma, D.J., and Moreno, G. (1988). The evolution of ecological specialization. Annu. Rev. Ecol. Syst. *19*, 207–233.

55. Ferry-Graham, L.A., Bolnick, D.I., and Wainwright, P.C. (2002). Using functional morphology to examine the ecology and evolution of specialization. Integr. Comp. Biol. *42*, 265–277. https://doi.org/10.1093/icb/42.2.265.

56. Hardy, C.R. (2006). Reconstructing ancestral ecologies: challenges and possible solutions. Divers. Distrib. *12*, 7–19. https://doi.org/10.1111/j.1366-9516.2006.00207.x.

57. Ricklefs, R.E. (2012). Species richness and morphological diversity of passerine birds. Proc. Natl. Acad. Sci. USA *109*, 14482–14487.

58. Clavel, J., Julliard, R., and Devictor, V. (2011). Worldwide decline of specialist species: toward a global functional homogenization? Front. Ecol. Environ. *9*, 222–228. https://doi.org/10.1890/080216.

59. Callaghan, C.T., Benedetti, Y., Wilshire, J.H., and Morelli, F. (2020). Avian trait specialization is negatively associated with urban tolerance. Oikos *129*, 1541–1551. https://doi.org/10.1111/oik.07356.

60. Greenberg, D.A., Pyron, R.A., Johnson, L.G.W., Upham, N.S., Jetz, W., and Mooers, A.Ø. (2021). Evolutionary legacies in contemporary tetrapod imperilment. Ecol. Lett. *24*, 2464–2476. https://doi.org/10.1111/ele.13868.

61. Verde Arregoitia, L.D., Blomberg, S.P., and Fisher, D.O. (2013). Phylogenetic correlates of extinction risk in mammals: species in older lineages are not at greater risk. Proc. Biol. Sci. *280*, 20131092. https://doi.org/10.1098/rspb.2013.1092.

62. Sayol, F., Wayman, J.P., Dufour, P., Martin, T.E., Hume, J.P., Jørgensen, M.W., Martínez-Rubio, N., Sanglas, A., Soares, F.C., Cooke, R., et al. (2024). AVOTREX: A global dataset of extinct birds and their traits. Global Ecol. Biogeogr. *33*, e13927. https://doi.org/10.1111/geb.13927.

63. Rabosky, D.L., and McCune, A.R. (2010). Reinventing species selection with molecular phylogenies. Trends Ecol. Evol. *25*, 68–74.

64. Hunter, J.P. (1998). Key innovations and the ecology of macroevolution. Trends Ecol. Evol. *13*, 31–36. https://doi.org/10.1016/S0169-5347(97)01273-1.

65. Miller, A.H., Stroud, J.T., and Losos, J.B. (2023). The ecology and evolution of key innovations. Trends Ecol. Evol. *38*, 122–131.

66. Oliveira, B.F., and Scheffers, B.R. (2019). Vertical stratification influences global patterns of biodiversity. Ecography *42*, 249. https://doi.org/10.1111/ecog.03636.

67. Scheffers, B.R., Phillips, B.L., Laurance, W.F., Sodhi, N.S., Diesmos, A., and Williams, S.E. (2013). Increasing arboreality with altitude: a novel biogeographic dimension. Proc. Biol. Sci. *280*, 20131581. https://doi.org/10.1098/rspb.2013.1581.

68. Tendler, A., Mayo, A., and Alon, U. (2015). Evolutionary tradeoffs, Pareto optimality and the morphology of ammonite shells. BMC Syst. Biol. *9*, 12. https://doi.org/10.1186/s12918-015-0149-z.

69. Schuech, R., Hoehfurtner, T., Smith, D.J., and Humphries, S. (2019). Motile curved bacteria are Pareto-optimal. Proc. Natl. Acad. Sci. USA *116*, 14440–14447. https://doi.org/10.1073/pnas.1818997116.

70. Burress, E.D., and Muñoz, M.M. (2023). Functional trade-offs asymmetrically promote phenotypic evolution. Syst. Biol. *72*, 150–160. https://doi.org/10.1093/sysbio/syac058.

71. Tanner, J.B., Dumont, E.R., Sakai, S.T., Lundrigan, B.L., and Holekamp, K.E. (2008). Of arcs and vaults: the biomechanics of bone-cracking in spotted hyenas (Crocuta crocuta). Biol. J. Linn. Soc. *95*, 246–255. https://doi.org/10.1111/j.1095-8312.2008.01052.x.

72. Jetz, W., Thomas, G.H., Joy, J.B., Hartmann, K., and Mooers, A.O. (2012). The global diversity of birds in space and time. Nature *491*, 444–448. https://doi.org/10.1038/nature11631.

73. Sheard, C., Neate-Clegg, M.H.C., Alioravainen, N., Jones, S.E.I., Vincent, C., MacGregor, H.E.A., Bregman, T.P., Claramunt, S., and Tobias, J.A. (2020). Ecological drivers of global gradients in avian dispersal inferred from wing morphology. Nat. Commun. *11*, 2463. https://doi.org/10.1038/s41467-020-16313-6.

74. Seki, Y., Schneider, M.S., and Meyers, M.A. (2005). Structure and mechanical behavior of a toucan beak. Acta Mater. *53*, 5281–5296.

75. Felice, R.N., Tobias, J.A., Pigot, A.L., and Goswami, A. (2019). Dietary niche and the evolution of cranial morphology in birds. Proc. Biol. Sci. *286*, 20182677. https://doi.org/10.1098/rspb.2018.2677.

76. Attard, M.R.G., Wilson, L.A.B., Worthy, T.H., Scofield, P., Johnston, P., Parr, W.C.H., and Wroe, S. (2016). Moa diet fits the bill: virtual reconstruction incorporating mummified remains and prediction of biomechanical performance in avian giants. Proc. Biol. Sci. *283*, 20152043.

77. Abourachid, A., Fabre, A.-C., Cornette, R., and Höfling, E. (2017). Foot shape in arboreal birds: two morphological patterns for the same pincer-like tool. J. Anat. *231*, 1–11.

78. Sayol, F., Steinbauer, M.J., Blackburn, T.M., Antonelli, A., and Faurby, S. (2020). Anthropogenic extinctions conceal widespread evolution of flightlessness in birds. Sci. Adv. *6*, eabb6095. https://doi.org/10.1126/sciadv.abb6095.

79. Jackson, H.D. (1970). Swimming ability of the Barn Swallow. Auk *87*, 20–57.

80. Hackett, S.J., Kimball, R.T., Reddy, S., Bowie, R.C.K., Braun, E.L., Braun, M.J., Chojnowski, J.L., Cox, W.A., Han, K.-L., Harshman, J., et al. (2008). A phylogenomic study of birds reveals their evolutionary history. Science *320*, 1763–1768. https://doi.org/10.1126/science.1157704.

81. Schliep, K.P. (2011). phangorn: phylogenetic analysis in R. Bioinformatics *27*, 592–593. https://doi.org/10.1093/bioinformatics/btq706.

82. Eugster, M.J.A., and Leisch, F. (2009). From Spider-Man to Hero - Archetypal Analysis in *R*. J. Stat. Softw. *30*, 1–19. https://doi.org/10.18637/jss.v030.i08.

83. Eugster, M.J.A., and Leisch, F. (2011). Weighted and robust archetypal analysis. Comput. Stat. Data Anal. *55*, 1215–1225. https://doi.org/10.1016/j.csda.2010.10.017.

84. Duong, T. (2007). ks: Kernel density estimation and kernel discriminant analysis for multivariate data in R. J. Stat. Soft. *21*, 1–16.

85. Uyeda, J.C., Caetano, D.S., and Pennell, M.W. (2015). Comparative analysis of principal components can be misleading. Syst. Biol. *64*, 677–689.

86. Rabosky, D.L. (2014). Automatic detection of key innovations, rate shifts, and diversity-dependence on phylogenetic trees. PLoS ONE *9*, e89543. https://doi.org/10.1371/journal.pone.0089543.

87. Rabosky, D.L., Grundler, M., Anderson, C., Title, P., Shi, J.J., Brown, J.W., Huang, H., and Larson, J.G. (2014). BAMMtools: an R package for the analysis of evolutionary dynamics on phylogenetic trees. Methods Ecol. Evol. *5*, 701–707. https://doi.org/10.1111/2041-210X.12199.

88. Revell, L.J. (2012). phytools: an R package for phylogenetic comparative biology (and other things): phytools: R package. Methods Ecol. Evol. *3*, 217–223. https://doi.org/10.1111/j.2041-210X.2011.00169.x.

89. Redding, D.W., and Mooers, A.Ø. (2006). Incorporating evolutionary measures into conservation prioritization. Conserv. Biol. *20*, 1670–1678. https://doi.org/10.1111/j.1523-1739.2006.00555.x.

90. Title, P.O., and Rabosky, D.L. (2019). Tip rates, phylogenies and diversification: what are we estimating, and how good are the estimates? Methods Ecol. Evol. *10*, 821–834. https://doi.org/10.1111/2041-210X.13153.

91. Kembel, S.W., Cowan, P.D., Helmus, M.R., Cornwell, W.K., Morlon, H., Ackerly, D.D., Blomberg, S.P., and Webb, C.O. (2010). Picante: R tools for integrating phylogenies and ecology. Bioinformatics *26*, 1463–1464. https://doi.org/10.1093/bioinformatics/btq166.

92. IUCN (2022). The IUCN Red List of Threatened Species. Version 2022-1 (IUCN).

93. Wood, S.N. (2011). Fast stable restricted maximum likelihood and marginal likelihood estimation of semiparametric generalized linear models.

J. R. Stat. Soc. B *73*, 3–36. https://doi.org/10.1111/j.1467-9868.2010.00749.x.

94. Hadfield, J.D. (2010). MCMC methods for multi-response generalized linear mixed models: The MCMCglmm R Package. J. Stat. Softw. *33*, 1–22. https://doi.org/10.18637/jss.v033.i02.
95. Birdlife International; NatureServe (2012). Bird species distribution maps of the world. Camb. UK NatureServe Arlingt (Birdlife International). http://www.birdlife.org/datazone/info/spcdownload.
96. Siddall, M., Rohling, E.J., Almogi-Labin, A., Hemleben, Ch., Meischner, D., Schmelzer, I., and Smeed, D.A. (2003). Sea-level fluctuations during the last glacial cycle. Nature *423*, 853–858. https://doi.org/10.1038/nature01690.
97. Ducatez, S., Tingley, R., and Shine, R. (2014). Using species co-occurrence patterns to quantify relative habitat breadth in terrestrial vertebrates. Ecosphere *5*, 1–12. https://doi.org/10.1890/ES14-00332.1.
98. Bird, J.P., Martin, R., Akçakaya, H.R., Gilroy, J., Burfield, I.J., Garnett, S.T., Symes, A., Taylor, J., Şekercioğlu, Ç.H., and Butchart, S.H.M. (2020). Generation lengths of the world's birds and their implications for extinction risk. Conserv. Biol. *34*, 1252–1261. https://doi.org/10.1111/cobi.13486.

Please cite this article in press as: Sayol et al., Ecophysical constraints on avian adaptation and diversification, Current Biology (2025), https://doi.org/10.1016/j.cub.2025.02.015

STAR★METHODS

KEY RESOURCES TABLE

REAGENT or RESOURCE	SOURCE	IDENTIFIER
Deposited data		
Data on species ecological traits generated for this study (n = 9,993 species)	This study	https://github.com/fsayol/BirdArchetypes
AVONET database for morphological data (n = 9,993 species), from Tobias et al.[28]	Tobias et al.[28]	https://doi.org/10.1111/ele.13898
Data on beak scans (n = 2,028 species), from Cooney et al.[31]	Cooney et al.[31]	https://doi.org/10.1038/nature21074
Software and algorithms		
R scripts to run all the analyses	This study	https://github.com/fsayol/BirdArchetypes

EXPERIMENTAL MODEL AND STUDY PARTICIPANT DETAILS

To quantify avian morphospace, we extracted linear measurements from the AVONET dataset[28] for all known extant birds (n = 9,993 species) aligned with a global phylogeny.[72] We then excluded from our analysis those species with missing information on any beak or body traits, respectively. For example, we removed Kiwis (*Apteryx*) from the body-trait analysis because they are arbitrarily assigned values of 0.1 mm for wing length. In total, we included n = 9,942 species for beak traits and n = 9,926 for body traits. For each species, we selected data for seven morphological traits known to predict trophic niche and locomotory behaviour in birds[2,73]: beak length, width and depth, tarsus length, tail length, wing chord and Kipp's distance (measured as the distance between the wing-tip and the tip of the first secondary feather). These traits were measured using a consistent protocol from a sample of 89,963 individuals (mean of 9 individuals per species) using museum specimens and live individuals captured and released in the field. Most of the variation in traits occurs among (98.25 %) rather than within (1.75 %) species, justifying the use of species mean trait scores.[28] While this dataset is of unparalleled scope, we acknowledge that it does not include other ecologically important aspects of morphology, including the material properties of the beak[74] or the morphology of the skull,[75] muscle[76] or foot.[77]

METHOD DETAILS

Principal components of morphological traits

To summarise variation in morphology across our species sample, we ran principal components analyses (PCA) on beak and body traits, separately. All trait variables were log-transformed and z-scaled before PCA. In each analysis, the first PC represents variation in size. In later analyses, we use body mass as a standard metric of body size but for beaks we use PC1 of the beak trait PCA (hereafter, we use beak size to mean scores on PC1). To examine morphological variation independent of size, we selected PCs representing shape (i.e. PC2 and PC3) and rescaled these to unit variance and a mean of zero prior to further analysis. Trait loadings for each beak and body trait are provided in Table S1. Measures of beak length, width and depth capture relative differences in beak dimensions but effectively assume a conical shaped beak. To ensure our results were not artefacts or treating beak shape in this simplistic way, we repeated our analysis using the first and second PC axis from beak shape measurements for 2028 species based on a Procrustes superimposition of landmarked 3D beak scans.[31]

Feeding techniques and foraging niches

The experimental data required to objectively score beak functions is generally lacking so we used a simplified system based on literature evidence to score the importance of three different beak physical tasks (crush, engulf and reach). To provide a first global characterisation of the relative importance of these tasks, we developed a new dataset describing the % used of 10 broad feeding techniques: plucking, crushing, tearing, hammering, spearing, probing, sweeping, filtering, grazing and engulfing (see Tables 1 and S3). To efficiently score the % use of each beak feeding technique for all ~10,000 bird species, we performed a multi-step approach that assigned a feeding technique to each of the 32 foraging niches recognized for birds[2] (See Tables 1 and S4) for each family of birds (n = 194 families). Morphology and ecology are often strongly conserved at the family level, but we also subdivided certain families into genera or species when there was variability in the assignment of feeding technique to a foraging niche within families (see examples below).

For each family, we used textual descriptions in the literature to identify the feeding techniques corresponding to each foraging niche used by the species in that family. For this, we used an existing global database that provides species level scores of the relative use of 32 different foraging niche categories,[2] each of which describes a combination of resource type (e.g. 'invertivore'), foraging behaviour (e.g. 'glean') and habitat (e.g. 'ground'). For example, both kiwis (*Apterygidae*) and landfowl (*Phasianidae*) are assigned

Please cite this article in press as: Sayol et al., Ecophysical constraints on avian adaptation and diversification, Current Biology (2025), https://doi.org/10.1016/j.cub.2025.02.015

to the 'Invertivore glean ground' foraging niche but utilise different feeding techniques, 'probing' and 'plucking' respectively. We note that while all species within a given family will receive the same beak feeding technique score for a particular foraging niche, the total use of a given beak feeding technique can vary across species in that family due to differences among species in the use of each foraging niche. For example, while all hummingbirds (*Trochilidae*) are scored as using a 'probing' feeding technique when foraging for nectar, the % contribution of 'probing' to a species' diet will vary as some species also obtain resources through other foraging niches (e.g. 'Invertivore aerial screening', whereby invertebrates are caught while the bird is in continuous and prolonged flight) which involve different feeding techniques (e.g. 'plucking').

Scoring beak-related physical tasks

To translate from beak feeding techniques to physical tasks, we scored the relative importance of the three different physical tasks (crush, reach and engulf) for each of the feeding techniques birds employ (Table S3). While subjective, our scoring system is designed to capture what is expected to be the primary selective pressure associated with each technique. For example, 'crushing' is a technique used for breaking open hard resources such as shells, seeds and nuts, and was assigned a score of 1 for 'crush' (and 0 for 'reach' and 'engulf'). In contrast, 'probing' involves the relatively slow or gentle insertion of the beak into a crevice or sediment to extract food and received a score of 1 for 'reach'. 'Engulfing' involves maximising the open-mouth surface area for filtering plankton[46] or capturing moving aerial insect prey[47] respectively and received a score of 1 for 'engulf'. Other feeding techniques likely rely on multiple physical tasks. For instance, the use of a 'hammering' technique to obtain hidden food (e.g. within dead wood) requires both a high resistance against fracturing but also reach to obtain the excavated prey and so was assigned a score of 0.5 for 'crush' and 0.5 for 'reach'. For each feeding technique, we scored the relative importance of each task from 0 to 1 in 0.25-unit intervals, with the exception of 'plucking' which was given an equal weight across tasks. With these scores, the importance of each physical task to each species was calculated by multiplying the importance score for a feeding technique by the % use of that technique.

Scoring body-related physical tasks

Scoring the importance of different locomotory modes for each species is challenging because quantitative data on the proportion of time or resources captured using different movements is not available for many species at a global scale. We therefore developed a simple system for translating our existing species level database[2] describing the relative use of 32 foraging niche categories into scores that capture the requirement to fly, swim or walk (See Table S4). We acknowledge that each of these coarse categories encompass a variety of different movements. For example, our 'walk' task includes walking, running, hopping and climbing. The 'swim' task variously includes plunge diving, dipping, pattering, wading, sitting on the water's surface and swimming under water. The 'fly' task includes such manoeuvres described in the literature as hawking, sallying and gliding. Here our aim was to summarise this variety in the broadest terms corresponding to use of different physical environments. For each foraging niche, we scored the relative importance of each task from 0 to 1 in 0.25-unit intervals.

Except for the very small number of flightless species (n = 60 species),[78] almost all birds make use of aerial movement during foraging or when not foraging (e.g. when dispersing between foraging sites or migrating). The vast majority of species are able to walk and most probably have some capacity to swim. Rather than giving (almost) all species an arbitrarily small score for these tasks, we set all physical tasks that are of only marginal importance to foraging to zero. For example, species exclusively using flight (e.g. 'Invertivore aerial screening') received a 'fly' score of 1 even though most of these species have some walking, and even swimming, ability.[79] Similarly, foraging niches that involve searching for food entirely on the ground (e.g. 'Invertivore glean ground' or 'Herbivore ground') received a 'walk' score of 1, even though most of these species also fly. Foraging niches that only involve swimming or diving during feeding, received a 'swim' score of 1 even though many of these species can also walk and/or fly. Some foraging niches clearly involve multiple physical tasks. For instance, the 'Invertivore glean elevated' niche that includes species predominantly feeding in trees can be considered to use a combination of flight between branches and movement across these branches (e.g. walking, hopping, hanging, climbing), and hence is assigned a score of 0.5 for fly and 0.5 for walk. Similarly, species that plunge into the water to catch prey, which require both flying and swimming during foraging, are assigned a score of 0.5 for fly and 0.5 for swim locomotion. With these scores for each foraging niche, the importance of each physical task to each species was calculated by multiplying the importance score for a foraging niche by the % use of that niche by each species. The scoring system for translating between foraging niches and locomotory tasks is provided in Table S4. Since these scores are subjective, they are intentionally coarse to acknowledge this uncertainty.

Phylogenetic trees

To understand the evolutionary dynamics of functional specialization and its influence on a species' capacity to respond to environmental change, we used the time-calibrated molecular BirdTree phylogeny[72] based on the Hackett backbone topology.[80] We downloaded a distribution of 100 complete phylogenies, including species inserted on the basis of taxonomy because they lacked genetic data (n = 9,993 species) and computed the maximum clade credibility (MCC) of the complete phylogeny using the R package 'phangorn'[81]. We also downloaded phylogenetic trees that included only species with genetic data (n = 6,670 species) for use in the trait reconstructions during the analyses of directionality of trait evolution. In this case, the phylogenetic trees were rate-transformed to account for heterogeneity in rates of trait evolution across the tree (See details below).

Please cite this article in press as: Sayol et al., Ecophysical constraints on avian adaptation and diversification, Current Biology (2025), https://doi.org/10.1016/j.cub.2025.02.015

QUANTIFICATION AND STATISTICAL ANALYSIS

Null models of beak morphospace volume and shape

We quantified the volume and shape of the 3D beak morphospace occupied by species defined by log-transformed length (L), width (W) and depth (D) measurements. Morphospace volume was quantified using a minimum convex hull. Our PC analysis indicates that size is the main axis of beak variation (Table S1). To intuitively quantify the magnitude of variation in observed beak sizes, we quantified the beak volume of each species, assuming beaks are conical in shape (beak volume = Pi x 1/3 x L x D x W). We then calculated the difference between the $\log_{10}$ transformed minimum and maximum beak volume. While almost perfectly correlated with beak PC1 ($r > 0.99$), the non-arbitrary scale of beak volume enables us to quantify the order of magnitude difference between the smallest and largest beaks (Figure S1B). We compared the observed range of beak volumes to that which is geometrically possible assuming extreme hypothetical trait combinations combining either the minimum or maximum values of each of length, width and depth. In all other analyses, where the arbitrary scale of PC axes is not important, we use PC1 as our index of beak size.

Following the methods of Diaz et al.,[1] we compared occupied morphospace volume (i.e., the space occupied in a 3D morphospace) and the variation in beak volume to that expected under null models that make contrasting assumptions about how species are distributed throughout trait space (Figure S1). Null model 1 assumes that there are no correlations among beak dimensions or trade-offs so that species can evolve extreme trait combinations with equal probability as central trait values. According to this null model, beak morphospace would approximate a cube. To simulate this, we sampled uniformly spaced values within the observed bounds of each trait axis independently. Null model 2 also assumes that each beak dimension varies independently, but that natural selection limits the exploration of extreme trait combinations, resulting in an approximately spherical morphospace. We implemented two variants of Null model 2. Null model 2.1 maintains the observed distribution of values along each trait dimension but randomly shuffles these independently across species, thus removing any covariation among trait dimensions. Null model 2.2 assumes a uniform distribution of values along each trait dimension but constrained these values to occur within a sphere of radius equal to half the mean range occupied by each trait dimension. The difference in expected occupied morphospace volume and beak volume variation between Null model 2.1 and Null model 2.2 was minor (Figure S1), indicating that the distribution of values within the observed range of each trait dimension has a relatively minor effect on expected morphospace occupancy. For each null model we performed 100 replicate simulations.

Archetypal analysis of beak and body shape

To formally describe the shape of beak morphospace defined by PC2 and PC3 we applied two different approaches. First, we used an archetypal analysis implemented in the R package 'archetypes'[82]. This approach aims to identify irregular polygons described by k vertices or 'archetypes' such that the distribution of species trait values can be well represented as convex combinations of these archetypes. For k vertices, the algorithm randomly selects an initial position for each vertex and then iteratively explores different vertex positions, trying to minimise the residual sum of squares (RSS) between the position of each species in trait space and the boundaries of the polygon. The original archetype algorithm,[82] requires these vertices to lie on the boundary of the convex hull enclosing the observations, making this method sensitive to extreme observations. Because we were interested in identifying the polygon shape that best describes the majority of bird forms, we used a 'robust archetype' analysis that downweighs the importance of extreme values.[83] We compared the fit of polygons with different numbers of vertices, from k=3 to 7 (Figure S2). Because the procedure for optimising polygon fit is stochastic, for each value of k we repeated the analysis 100 times and from across the replicates calculated the median and 95% CI in RSS.

The best-fitting polygons identified through an archetype analysis can take irregular forms so that shapes with more vertices will always describe the observed data better (Figure S2). For example, a polygon with 4 vertices can be constructed that will more closely fit the observed boundaries of morphospace, even if this shape is largely triangular in form (i.e. two of the vertices may be close together). We therefore developed a new shape-fitting algorithm based on regular polygons, with edges of equal length (Figure S3). We systematically explored polygons from 3 to 7 vertices and finally a polygon with $n = 360$ vertices approximating a circle. A circle is expected either when there are no constraints on morphospace or when there are a very large number of trade-offs between trait axes. Our algorithm systematically varied polygon position, area and angle of rotation, allowing us to identify the polygon where the distance between the boundary of the polygon and the boundary of observed morphospace was minimised. The boundary of observed morphospace was calculated using multivariate kernel density estimation in the R package "ks"[84]. The kernel was a multivariate normal distribution for each species centred on the trait values for each species with the optimal bandwidth selected using the *Hpi* function. We used the contour containing 90% of the total density of species as the boundary of empirical morphospace. The use of the 90% contour avoids estimates of morphospace shape being dominated by the small number of species with extreme traits. Because of the greater flexibility (i.e. allowing irregular shapes) we used the 'robust archetype' analysis to identify the location of archetypes and used our new regular polygon fitting approach, which is more conservative (i.e. is more likely to penalise shapes with many vertices), to confirm the number of vertices required to describe morphospace.[83]

Finally, we built two different sets of null models for beak and body shape, to test whether the skewed distribution of morphological traits or the asymmetric shape of the phylogenetic tree alone could cause a triangular shape of the morphospace (Table S2). First, we randomised each trait column in our dataset to break the correlation of traits within species (RND null model). Second, we simulated traits according to a Brownian motion model of evolution (BM null model). For this, we used the observed variance-covariance matrix (vcv) of raw traits in our dataset to simulate the evolution of new raw traits on the same phylogenetic tree, based on the vcv, using the

Please cite this article in press as: Sayol et al., Ecophysical constraints on avian adaptation and diversification, Current Biology (2025), https://doi.org/10.1016/j.cub.2025.02.015

ratematrix and *sim.char* functions from "geiger" R-package. The simulations were repeated 100 times. We then used the randomised (RND null model) and the simulated (BM null model) raw traits to re-run a PCA from which we extracted PC2 and PC3 and to which we fit regular polygons with different numbers of vertices (3, 4, 5, 6, 7 and 360). The two different null models were repeated 100 times for beak and body shape, and we calculated the proportion of simulations in which each polygon shape (i.e. number of vertices) was best supported.

Correspondence between archetypes and physical tasks

We visualised how feeding techniques and physical tasks are distributed throughout morphospace by overlaying a regular grid and then summing the relative % score of each technique/task across the species within each cell. Because some techniques/tasks are relatively more commonly used than others (e.g. there are many more terrestrial species specialised for walking than aquatic species specialised for swimming), we quantified the proportional importance of each technique/task in a cell weighted by the total % use of each technique/task across all species. Thus, our maps showing techniques/tasks across morphospace indicate regions where each technique/task is relatively highly represented accounting for its overall prevalence across birds (Figure 2).

To formally test whether specialization in a physical task is higher closer to the vertices of the Pareto front we used beta regression. For each focal archetype, we rescaled the distance of species from that archetype to between 0.001 and 0.999. We then estimated the slope of the relationship between distance as the response variable and the % use of that physical task as the predictor. We include a quadratic predictor term in the model to allow for non-linear responses (Figure 3).

Our analysis of physical tasks is based on coarsely defined scores which, while informed by basic physical principals, are not based on actual measurements of the functional performance of different beak shapes. Experimentally derived data on bite force (n = 77 species, [43]) and bite speed (n = 18 species, [44]) is available for a small subset of species allowing us to examine how these metrics of performance vary across morphospace. Our hypothesis is that species where crushing is inferred to be the primary physical task (Archetype 1) should have higher bite force, but at the expense of a slower bite speed.[14,43] To test this, we fitted a linear model to estimate the slope of the relationship between bite force (log-transformed) or bite speed as response variables, and beak size (i.e. beak PC1) and distance to Archetype 1 (from beak shape archetypes) as predictors. As expected, bite force increased with beak size (β_{PC1} = 1.13 ± 0.98, p<0.001) and decreased with the distance from Archetype 1 (β_{dA1} = -0.40 ± 0.08, p<0.001). Together, beak size and proximity to Archetype 1 explain a substantial proportion of the variation in bite force across species (R^2 = 0.66). Bite speed is independent of beak size (p>0.05) and increases strongly with distance from Archetype 1 (β_{dA1} = 0.19 ± 0.04, p<0.001). Distance from Archetype 1 explains 61% of the variation in bite speed. Thus, quantitative data on beak performance support the hypothesis that Archetype 1 corresponds to specialization for crushing food items, but at the expense of efficiently capturing mobile resources with the capacity to flee.

Sensitivity analyses

A potential criticism of our analysis is that it is based on simple linear measurements of beak length, width and depth, which ignores additional aspects of shape variation (e.g., curvature). It is possible that the PC axes we use may therefore not necessarily align with the primary axes of beak shape variation. We tested this by repeating our analysis on a subsample (n = 2026 species) using the first two shape axes derived from 3D beak scans that measure the full complexity of shape, including curvature.[31] These results confirmed that a triangular shape (i.e. three archetypes) was the best supported model for beak shape morphospace, and that distance from the vertices of this triangle reliably predict the relative importance of the different beak physical tasks (Figure S4A). This makes sense because the two primary shape axes derived from 3D beak scans are strongly aligned with our PC2 (r = 0.89) and PC3 (r = 0.37), confirming that our simple linear measurements reliably capture the main dimensions of beak shape variation. We acknowledge that including additional dimensions of shape that account for less morphological variation would likely reveal further trade-offs.

In all the analyses, we used standard PCA rather than Phylogenetic PCA (PPCA) because the latter can only reliably account for phylogenetic non-independence when traits have evolved under a simple Brownian motion process.[85] However, to test whether the observed trade-offs potentially reflect some aspects of within-clade variation rather than universal constraints, we repeated our analysis using the second and third axis derived from PPCA (PPC2 and PPPC3) and found that the patterns remain the same (Figures S4B and S4C). That is, for both beak and body shape, there is an overall triangular shape of morphospace and species specialized to single physical tasks concentrate near the vertices. In some cases, the axes are flipped (i.e. species with high values on Body PC3 have low values of Body PPC3 and vice versa) or slightly rotated. However, this does not alter the shape of morphospace.

Another potential critique is that our analysis of archetypes focuses on trade-offs in a two-dimensional beak morphospace that ignores variation in beak size, a key trait in predicting avian ecological niches.[2] Including variation in beak size, could potentially identify different morphospace geometries and archetypal forms. To test this, we repeated our archetype analysis using a 3D morphospace including beak PC1, together with PC2 & PC3. We calculated the best supported polyhedrons with 4 and 5 archetypes and then projected the position of these archetypes onto the original 2D plane defining beak shape (Beak PC2 and PC3). We found that an overall triangular shape is still observed, as newly identified archetypes are in similar positions to those we have previously identified, and are only separated across the size axis (Figure S5A). In other words, they represent large and small versions of each archetype. For instance, in beak morphospace, the archetype of relatively long beaks, corresponding to the reach task (A2), is duplicated into a large (e.g. ibis) and small (e.g. hummingbird) beak size when 4 and 5 archetypes are fitted, whereas the archetype corresponding to the engulf task (A3) is duplicated into large (e.g. frogmouths) and small (e.g. swallows) beak size when 4 archetypes are fitted. We obtained similar results when fitting archetypes to a 3D body morphospace including body PC1, with archetypes projected on to

Please cite this article in press as: Sayol et al., Ecophysical constraints on avian adaptation and diversification, Current Biology (2025), https://doi.org/10.1016/j.cub.2025.02.015

the original 2D space forming a triangle (Figure S5B). This is consistent with the pareto front theory that archetypes identified in one plane are indicative of constraints closer to that particular combination of traits, irrespective of how many more axes are added.[17]

We performed sensitivity analyses to assess whether the correspondence between archetypes and physical tasks was robust to the subjective scoring of physical tasks. For the beak-related physical tasks, we identified all cases where a feeding technique had an importance score for a focal task between 25-75% and we upweighted the score to 75%. To maintain a total score of 100% for each feeding technique, we proportionally reduced the importance scores for the other tasks (dividing equally if two tasks were involved). We then recalculated the physical task scores for each species and the distribution of each task across morphospace. This procedure was repeated for each task (Figures S6A–S6C). A similar sensitivity analysis was performed for body shape and the associated task scoring (Figures S6D–S6F).

Directionality in trait evolution

To explore the directionality of beak and body shape evolution between each node in the avian phylogenetic tree, we performed an ancestral trait reconstruction for each of the PC axes of beak and body shape. Because trait reconstructions can be sensitive to tree topology and rate heterogeneity across the tree, we ran the reconstruction analysis on rate-transformed phylogenies that include species with genetic data (n = 6670 species). First, we fit a variable rate trait evolution model in BAMM[86] for PC2 and PC3 axes separately (for both beak and body shape) allowing variation in rates across branches of the tree and over time. Priors were set as 50 for the expected number of rate shifts (recommended for trees >5000 species), 0.25 for the initial evolutionary rates (betaInitPrior) and 0.1 for the distribution of the magnitude of the rate shift change (betaShiftPrior). We ran the analysis for 5,000,000 generations, with a thinning interval of 10,000 and a burn-in of 100,000. We then used the output to create a rate-transformed phylogeny for each PC using the "getMeanBranchLengthTree" function from the 'BAMMtools' R package,[87] where each branch length is multiplied by the mean rate of evolution from across the inferred distribution of rates. Then, we used the *fastAnc* function from the 'phytools' R package[88] to infer the ancestral values of each PC axis, using the corresponding rate-transformed tree. Finally, we used the inferred ancestral values to calculate the overall direction of trait evolution across all phylogenetic branches, and specifically whether this was 'inward' towards the centroid of morphospace or 'outward', away from the centroid. To do this, we calculated the difference in the distance from the centroid of morphospace between each ancestor and each of its two descendants, and report the ratio of inward and outward branches. We next calculated how the direction of trait evolution varies locally across morphospace by overlaying a regular grid and identifying the phylogenetic branches intersecting each grid cell based on the inferred morphological position of the ancestor and descendent node. We then calculated the circular mean and variance (V_{obs}) in the angle of trait evolution.

A net outward flow of lineages away from the centroid of morphospace (O) could be expected for geometric reasons. This point is best explained with the logic of Fisher's geometric model of adaptation.[53] Consider an ancestral node, denoted by point A in morphospace lying on the boundary of a circle centred at O. When the distance evolved (r) from A to its descendent node is infinitesimally small, then this is equally likely to move the lineage towards or away from O. In contrast, if r is greater than the diameter (d) of the circle, then regardless of the direction of evolution, the lineage will move away from O.

This simple geometric model indicates that the number of lineages moving outwards, away from the centroid of morphospace, is likely to exceed those moving inwards even if lineages are evolving in random directions.

To formally test whether the inferred directionality of trait evolution is different to that expected if traits had evolved in random directions, we first compared the inferred proportion of outward trajectories to that expected under a multi-rate Brownian motion (BM) model of evolution. We used the *fastBM* function from the R package *phytools*[88] to simulate the evolution of traits along the branches of rate-transformed trees generated using the rates of evolution inferred from our observed trait data. We repeated this 100 times and for each replicate simulation conducted an ancestral state reconstruction and calculated the proportion of outward and inward branch trajectories. We then rejected the null model if the observed ratio of outward versus inward trajectories was outside the 95% C.I. of the null model distribution. We report the % of times where branches evolved outwards and the P-value refers to the proportion of times where the observed ratio of outward evolution is greater than the ratio of the simulated data. The same analysis was performed using the beak shape axes and the body shape axes independently.

We next tested for non-random directionality locally using an alternative procedure which is necessary because in any given null model simulation a grid cell may fail to contain any inferred branches or contain far more or fewer than is inferred for the observed data due to the model of random trait evolution. Our null model of local directionality therefore used the following steps. First, for each simulation run we calculated the variance in the inferred direction of evolution (V_{sim}) for each grid cell. Second, we plotted how V_{sim} varies according to the number of branches intersecting a cell (NB_{sim}). For this, we pooled values of V_{sim} and NB_{sim} across simulation runs. Third, we identified the boundary describing the minimum V_{sim} expected for a given value of NB_{sim} using a quantile regression and the 5% quantile (i.e. 1-tailed test). Fourth, given the number of branches in our empirical data inferred to intersect each cell (NB_{obs}), we identified values of V_{obs} that were lower than expected under the null model. A significantly lower variance indicates that co-occurring branches tend to evolve in a more consistent direction than expected under a null model of trait evolution.

Mapping speciation rates and extinction risk across morphospace

To explore how different regions of morphospace are associated with variation in speciation rate, we used the species level diversification rate (DR) metric.[72] This is calculated as the inverse of the equal splits (ES) metric of evolutionary isolation[89] and although originally considered a measure of net diversification, it more closely approximates speciation rate.[90] We used the function "evol.distinct" from the R package 'picante'[91] to calculate the DR of each species across the complete BirdTree phylogeny. We then

Please cite this article in press as: Sayol et al., Ecophysical constraints on avian adaptation and diversification, Current Biology (2025), https://doi.org/10.1016/j.cub.2025.02.015

identified those species in the top DR quartile (i.e., top 25%) as having high speciation rates (1), with the remaining species scored as having relatively low (0) speciation rates. To explore how different regions of morphospace are associated with variation in extinction risk, we used species threat status from the IUCN Red List (version 2022-1).[92] We converted threat status into a binary classification by considering species treated as Least Concern (LC) as not threatened (0) and all other classifications (Near Threatened [NT], Vulnerable [VU], Endangered [EN], and Critically Endangered [CR]) as threatened (1). Species classified as Data Deficient (DD) were excluded (n = 38). We modelled both speciation rate (1 vs 0) and extinction risk (1 vs 0) as a function of the position of species in morphospace using a generalised additive model (GAM) with a binomial error distribution implemented in the R package 'mgcv'[93]. Specifically, we used the position of species in beak or body shape morphospace (PC2 and PC3) to predict the relative incidence across morphospace of lineages with high speciation rates and high extinction risk, respectively. Additionally, GAMs were used to predict (1) invertivore gleaner specialists (1 vs. 0), (2) beak task specialization (1 vs. 0), and (3) body task specialization (1 vs. 0), based also on morphospace position. Invertivore gleaner specialists were defined as species with a foraging niche categorized as "Invertivore glean elevated" $\geq$ 60%). Beak and body task specialists were species specializing in a single task (i.e., focusing on one of three tasks at $\geq$ 60%).

To formally test the effect of functional specialization (i.e. phenotypical optimization for a single task) on speciation rates and extinction risk, we fitted species-level Bayesian linear mixed models accounting for the phylogenetic non-independence of species using the R package 'MCMCglmm'[94]. For speciation rate, we modelled DR (log-transformed) using a normal distribution (Gaussian). We modelled extinction risk (1= Threatened; 0 = Non-threatened) as a binary-response with a probit link (ordinal). In both models, the predictors were the degree of functional specialization in beak and body shape, calculated as the distance to the nearest beak and body shape archetype, respectively. We also included other factors expected to influence extinction risk and speciation rate, including degree of insularity, habitat breadth and generation length (log-transformed). To avoid issues arising due to collinearity, body mass was not included as it was highly correlated with generation length (Pearson's r=0.84) and might cause co-linearity problems. The degree of insularity was assessed from the BirdLife International distribution maps.[95] We classified each species as insular (value of 1) when occurring year round on oceanic islands that did not reconnect to the continent when sea levels changed during glacial periods (considering the minimum level of 120 m below current level).[96] Species that occur on continental or land bridge islands, that do reconnect with continents were given a value of 0.5, whereas species that occur on continents were given a value of 0. Habitat breadth was obtained from Ducatez et al.,[97] which employs a multiplicative beta diversity index derived from the presence/absence of species along 82 different habitat subtypes from the IUCN.[92] Generation length was obtained from Bird et al.[98] Each model was run for 110,000 iterations (with a 10,000 burn-in). The thinning interval was set to 100, resulting in a posterior distribution of 1,000 samples, and sufficient to ensure that the autocorrelation of samples was <0.1. The models include the phylogenetic effects as a random factor, using a maximum clade credibility tree (MCC) from the posterior sample of full trees.